Journal of Experimental Botany, Vol. 73, No. 11 pp. 3637–3650, 2022
https://doi.org/10.1093/jxb/erac078 Advance Access Publication 26 February 2022

RESEARCH PAPER

NaCl affects photosynthetic and stomatal dynamics by osmotic effects and reduces photosynthetic capacity by ionic effects in tomato

Yuqi Zhang[1,2], Elias Kaiser[2], Tao Li[1,*], and Leo F.M. Marcelis[2]

[1] Institute of Environment and Sustainable Development in Agriculture, Chinese Academy of Agriculture Sciences, Beijing, China
[2] Horticulture and Product Physiology, Department of Plant Sciences, Wageningen University, Wageningen, The Netherlands

* Correspondence: litao06@caas.cn

Received 9 August 2021; Editorial decision 23 February 2022; Accepted 25 February 2022

Editor: Tracy Lawson, University of Essex, UK

Abstract

NaCl stress affects stomatal behavior and photosynthesis by a combination of osmotic and ionic components, but it is unknown how these components affect stomatal and photosynthetic dynamics. Tomato (*Solanum lycopersicum*) plants were grown in a reference nutrient solution [control; electrical conductivity (EC)=2.3 dS m^{-1}], a solution containing additional macronutrients (osmotic effect; EC=12.6 dS m^{-1}), or a solution with additional 100 mM NaCl (osmotic and ionic effects; EC=12.8 dS m^{-1}). Steady-state and dynamic photosynthesis, and leaf biochemistry, were characterized throughout leaf development. The osmotic effect decreased steady-state stomatal conductance while speeding up stomatal responses to light intensity shifts. After 19 d of treatment, photosynthetic induction was reduced by the osmotic effect, which was attributable to lower initial stomatal conductance due to faster stomatal closing under low light. Ionic effects of NaCl were barely observed in dynamic stomatal and photosynthetic behavior, but led to a reduction in leaf photosynthetic capacity, CO_2 carboxylation rate, and stomatal conductance in old leaves after 26 d of treatment. With increasing leaf age, rates of light-triggered stomatal movement and photosynthetic induction decreased across treatments. We conclude that NaCl impacts dynamic stomatal and photosynthetic kinetics by osmotic effects and reduces photosynthetic capacity by ionic effects.

Keywords: Fluctuating light, ionic stress, osmotic stress, photosynthesis, salt stress, stomatal conductance, tomato.

Introduction

Salt stress, induced by soil salinity, is a major abiotic stress in crop production. Over 1 billion hectares of farmland in more than 100 countries are affected by high salinity, and this area is growing (FAO/ITPS, 2015). Photosynthesis is a major determinant of plant growth and yield, and is strongly affected by salt stress (Chaves *et al.*, 2011). Reduced stomatal conductance (g_s) is usually considered to increase CO_2 diffusive limitations to photosynthesis (X. Wang *et al.*, 2017). In nature, plants often experience salt stress concomitantly with highly dynamic light intensities, also termed fluctuating light (FL), due to variations of the solar angle, cloud movement, wind-induced leaf fluttering, and shading from overlapping leaves and neighboring

plants (e.g. Pearcy, 1990; Wang *et al.*, 2020). Stomatal opening and closure in response to changes in irradiance affect photosynthesis under FL (McAusland *et al.*, 2016; Qu *et al.*, 2016; Faralli *et al.*, 2019; Papanatsiou *et al.*, 2019), which can also be strongly affected by salt stress. Therefore, knowledge about stomatal and photosynthetic behavior in salt-stressed plants under FL can be useful for crop management and breeding strategies to improve yields under salt stress, but so far this has received little attention.

In nature, changes in leaf net photosynthetic rate (A) lag behind changes in light intensity (Pearcy *et al.*, 1996). For example, when a leaf in the shade is suddenly exposed to high light intensity, the leaf requires a period of between several seconds and tens of minutes to regain maximum photosynthetic efficiency (Kimura *et al.*, 2020). This process is called photosynthetic induction. Slow photosynthetic induction has been estimated to lead to remarkable losses of 10–50% (Morales *et al.*, 2018; Pearcy *et al.*, 1997; Taylor and Long, 2017) in daily potential carbon gain, relative to a hypothetical immediate response of photosynthesis to changes in light intensity. Previously, we demonstrated that photosynthetic induction after dark–light transitions was strongly inhibited in NaCl-stressed tomato leaves after 7–9 d of NaCl application, which was largely due to increased transient stomatal limitation (Zhang *et al.*, 2018). Therefore, salt stress down-regulated photosynthesis much more strongly under FL than under constant or steady-state light conditions (Zhang *et al.*, 2018; Zhang *et al.*, 2020). We also found that NaCl-stressed tomato leaves showed a significantly shorter time for g_s to reach the final value after dark–light transitions, as well as a faster decrease in g_s after transitions from high to low light intensity (Zhang *et al.*, 2018). However, effects of salt stress depend on the duration of salt exposure, and leaf aging itself could interfere with the effects of salt stress on its photosynthesis. Therefore, it is useful to investigate how the duration of salt stress interacts with the leaf developmental stage, both of which may affect dynamic stomatal and photosynthetic behavior.

Salt stress affects plants mainly through two effects, the osmotic and the ionic effect, which are often viewed as working on different timelines (Munns and Tester, 2008). The osmotic effect impacts plants immediately after an increase in soil salinity; it results from a reduction of the osmotic potential at the root surface due to a high concentration of ions in the soil/nutrient solution, making it more difficult for roots to take up water (Castillo *et al.*, 2007; Munns and Tester, 2008). The osmotic effect can decrease cell expansion rates in growing and young leaves, as well as impede stomatal opening, in a similar manner to drought stress (Munns and Tester, 2008; Rengasamy, 2010*a*; Shabala and Munns, 2017). The ionic effect, on the other hand, appears after a longer exposure to salt stress (days to weeks) when ions (e.g. Na^+ and Cl^-) accumulate to toxic concentrations in transpiring leaves. This accumulation can cause an ionic imbalance in plant cells (Shabala and Munns, 2017), severely inhibit photosynthetic enzymes, and lead to early senescence of old leaves (Munns and Tester, 2008; Richter *et al.*, 2019). The ionic effect may add to the osmotic effect, but may also interact with it. NaCl is the most soluble and widespread salt (Munns and Tester, 2008). To understand how NaCl stress affects dynamic stomatal and photosynthetic behavior under FL, it is necessary to know to what extent they are affected by either of these effects under prolonged exposure to NaCl.

In this study, we aimed to disentangle the osmotic and ionic effects of NaCl on dynamic stomatal behavior and photosynthetic performance during leaf development. We hypothesized that (i) the osmotic effect of NaCl would occur first, leading to decreased g_s as well as a faster g_s response to dynamic light; (ii) the ionic effect of NaCl would appear later, further reducing g_s under dynamic light; and (iii) both osmotic and ionic effects of NaCl would decrease accumulated photosynthesis rate under dynamic light. Tomato (*Solanum lycopersicum*) was used in this study, as it is an important fruit crop worldwide (Heuvelink, 2018) and is widely cultivated in many countries that suffer from soil salinity (Ghorbani *et al.*, 2018). Tomato plants were grown in isosmotic solutions with and without NaCl. Plant growth, leaf acclimation traits, and steady-state and dynamic stomatal and photosynthetic performance were investigated.

Materials and methods

Plant material and treatments

Tomato (*Solanum lycopersicum* cv. Moneymaker) seeds were germinated in vermiculite. At 22 d after sowing (when the third true leaves started to appear), the roots were washed in tap water and seedlings were transplanted on to Styrofoam® sheets (~3 cm thick) that floated in a container with 7.6 litres of nutrient solution (Supplementary Fig. S1). The nutrient solution was constantly aerated using air pumps. Plants were grown in a climate-controlled room (3.0 × 2.2 × 3.1 m in length, width, and height) at ambient CO_2 partial pressure (maintained at ~480 μbar), day/night temperature of 25/20°C, and an average relative humidity of 70%. Plants were subjected to 200 μmol m^{-2} s^{-1} photosynthetic photon flux density (PPFD), measured at canopy level with a photoperiod of 16 h. Light was provided by red and white LEDs (Philips GreenPower deep red/white LED production modules, Eindhoven, The Netherlands; spectrum is shown in Supplementary Fig. S2).

Three days after transplanting, three salt treatments were applied (Supplementary Table S1): control solution [electrical conductivity (EC)=2.3 dS m^{-1}]; osmotic solution (EC=12.6 dS m^{-1}), with increased concentrations of macronutrients in the nutrient solution (macronutrients were increased in the same proportions as in the control solution and micronutrients were kept constant); and NaCl solution (EC=12.8 dS m^{-1}), in which 100 mM NaCl was added to the control solution. The EC of each solution was first calculated using a R script that was based on the Truesdell–Jones ion activity model (van Delden *et al.*, 2020) and later measured with a calibrated EC meter (Orion Star™ A329, Thermo Fisher Scientific, Waltham, MA, USA). The use of concentrated macronutrient solutions to separate the osmotic effect from the ionic effect of Na^+ and Cl^- was suggested by Termaat and Munns (1986), Rengasamy (2010*a*), and Tavakkoli *et al.* (2010). In the concentrated nutrient solution, all macronutrients were present in the same proportions as in the control solution, suggesting that any effects on the plant were due to osmotic effects rather than due to any single ion (Rengasamy, 2010*a*). Therefore, differences between plants grown in concentrated macronutrients and

the control solution were considered to be attributable to the osmotic effect, and differences between plants grown in concentrated macronutrients and in the NaCl solution were considered to be attributable to the ionic effect of Na^+ and Cl^-.

Concentrated macronutrients and NaCl were applied in 25% increments daily for 4 d sequentially to allow plants to slowly acclimate to the final concentrations. The pH and EC of each solution were monitored and adjusted daily: the pH was adjusted to 5.5–6.5 by the addition of 0.1 M H_2SO_4 or 0.1 M HNO_3, and the EC was adjusted by adding small amounts of deionized water to compensate for water loss through transpiration. All nutrient solutions were completely refreshed once per week.

The experiment was conducted three times in succession, and in each experiment there were 15 replicate plants per treatment. Measurements detailed below were repeated in two or three of the experiments. In order to follow single leaves throughout development, the third true leaf, counted from the bottom of the plant, was used for gas exchange and chlorophyll fluorescence measurements, and whole plants were destructively harvested at 6, 12, 19, and 26 d after treatments started (DAT). To avoid the development of shade-induced senescence, full light exposure of the third leaf was ensured throughout the experiment, by using bamboo sticks that blocked upper leaves from moving above the third leaf.

Photosynthetic gas exchange and chlorophyll fluorescence

Photosynthetic gas exchange and chlorophyll fluorescence measurements were performed using the LI-6400XT photosynthesis system (LI-COR Biosciences, Lincoln, NE, USA) equipped with a leaf chamber fluorometer (LI-COR part no. 6400-40, enclosed leaf area: 2 cm^2). Unless stated otherwise, all measurements were performed at a leaf temperature of approximately 25 °C, leaf-to-air vapour pressure deficit of 0.7–1.0 kPa, and flow rate of air through the system of 500 μmol s^{-1}. Irradiance was provided by a mixture of red (90%) and blue (10%) LEDs in the fluorometer. Peak intensities of red and blue LEDs were at wavelengths of 635 nm and 465 nm, respectively.

Light response curves of leaf photosynthesis

Leaves were adapted to 200 μmol m^{-2} s^{-1} PPFD and 400 μbar CO_2 partial pressure, until A was stable. Leaves were then exposed to a range of PPFDs (200, 150, 100, 50, 0, 200, 400, 600, 800, 1000, and 1500 μmol m^{-2} s^{-1}). Upon reaching steady-state conditions at each PPFD (10–15 min), gas exchange parameters were logged continuously (every 5 s) for 1 min, and averages of 12 values were used at each PPFD step. At each PPFD, a multiphase flash (MPF) chlorophyll fluorescence routine was executed to determine the fluorescence yield under actinic light (F_s), as well as maximum (F_m') and minimum (F_0') fluorescence, following recommended procedures (Loriaux *et al.*, 2013). Settings of the MPF were determined in a preliminary experiment: the measuring beam intensity was 1 μmol m^{-2} s^{-1}, maximum flash intensity was 7500 μmol m^{-2} s^{-1}, flash intensity decreased by 60% during the second phase of the MPF, and the durations of the three flash phases were 0.3, 0.7, and 0.4 s, respectively.

CO_2 response curves of leaf photosynthesis

CO_2 response curves should be obtained at saturating light intensity to determine the maximum carboxylation rate (V_{cmax}), electron transport rate (J), and triose phosphate use (TPU) (Sharkey *et al.*, 2007). A was near-saturated under 1500 μmol m^{-2} s^{-1} PPFD (Fig. 1A–D); thus, leaves were first adapted in the LI-6400XT leaf chamber to 1500 μmol m^{-2} s^{-1} PPFD and 400 μbar CO_2, until A was stable. Leaves were then exposed to a range of CO_2 partial pressures (400, 300, 200, 100, 75, 50, 400, 600, 800, 1000, 1200, and 1500 μbar). Upon reaching steady-state conditions at each CO_2 partial pressure (duration was 3–5 min per step, except the step from 50 μbar to 400 μbar, which took ~15 min), gas exchange parameters were logged continuously (every 5 s) for 1 min, and averages of 12 values were used.

Analysis of steady-state leaf photosynthesis

Data were corrected for leakage of CO_2 into or out of the cuvette, according to the LI-6400XT manual (version 6.2, LI-COR Biosciences). A non-rectangular hyperbolic function (Cannell and Thornley, 1998) was fitted to the light response curve, and parameters were derived including maximum net photosynthetic rate (A_{max}), dark respiration rate (R_{dark}), and apparent quantum yield (α). Average g_s across all PPFD values of the A/PPFD curves ($\bar{g}_s$) was calculated. The day respiration rate (R_d) was estimated to be 50% of R_{dark} (Sharkey, 2016). Mesophyll conductance (g_m) at 400 μbar CO_2 was calculated using the variable J method (Harley *et al.*, 1992). Using measured A/internal CO_2 partial pressure (C_i) curve values and fixed R_d and g_m values, V_{cmax}, electron transport rate at 1500 μmol m^{-2} s^{-1} PPFD (J_{1500}), and TPU were derived, using the Excel solver provided by Sharkey (2016).

Dynamic photosynthetic responses to step changes in irradiance

To assess the response of gas exchange and chlorophyll fluorescence to a step increase in PPFD, leaves were dark-adapted in the LI-6400XT leaf chamber for approximately 30 min, and F_0 and F_m were recorded. Then, irradiance was increased to 50 μmol m^{-2} s^{-1}, and leaves were kept at this PPFD until A and g_s were stable (~30 min). Then, PPFD was increased in a single-step change to 1500 μmol m^{-2} s^{-1} for 60 min (first induction phase), and A, g_s, and C_i were logged once per second. A PPFD of 1500 μmol m^{-2} s^{-1} was chosen to maximize the effects that NaCl may have on the rate of photosynthetic induction, as well as to test how plants cope with this high-light stress. F_s and maximum F_m' were logged every minute during the first 10 min of photosynthetic induction, and every 2 min thereafter.

To test the response of photosynthetic gas exchange to a period of shade, following the above measurements, PPFD was decreased to 50 μmol m^{-2} s^{-1} for 30 min. Then, PPFD was raised again to 1500 μmol m^{-2} s^{-1} for 10 min (second induction phase), and gas exchange was logged once per second.

Analysis of dynamic leaf photosynthesis

Transient responses of A, g_s, and C_i after step increases and decreases in light intensity were averaged over five data points to reduce measurement noise, using a moving average filter. Photosynthetic induction state was calculated after Zipperlen and Press (1997). The following parameters during the first photosynthetic induction phase were derived: (i) initial steady-state A under 50 μmol m^{-2} s^{-1} (A_i; mean value of 120 s before the increase in PPFD); (ii) final steady-state A under 1500 μmol m^{-2} s^{-1} (A_f; mean value of 120 s of full photosynthetic induction); (iii) photosynthetic induction state at 60 s after illumination (IS_{60}); (iv) the time required to reach 50% (t_{50}) and 90% (t_{50}) of full photosynthetic induction; and (v) average A during the first 300 s of photosynthetic induction (A_{300}). IS_{60}, t_{50}, and A_{300} were also calculated during the second induction phase. Because A did not reach steady state at the end of the second induction phase, A_f during the first induction phase was used for calculating IS_{60} and t_{50} during the second induction phase. Transient stomatal and non-stomatal limitations during photosynthetic induction were calculated after Zhang *et al.* (2018).

Modelling dynamic g_s responses to PPFD

To quantify the temporal response of g_s to a step change in PPFD, two empirical models (exponential model and sigmoidal model; Vialet-Chabrand *et al.*, 2017) were used. Based on the shape of the g_s response to a step increase in PPFD, the sigmoidal model was used:

$$g_s = \left(g_{sf} - g_{si}\right) e^{-e^{\left(\frac{\lambda - t}{k_i} + 1\right)}} + g_{si} \quad (1)$$

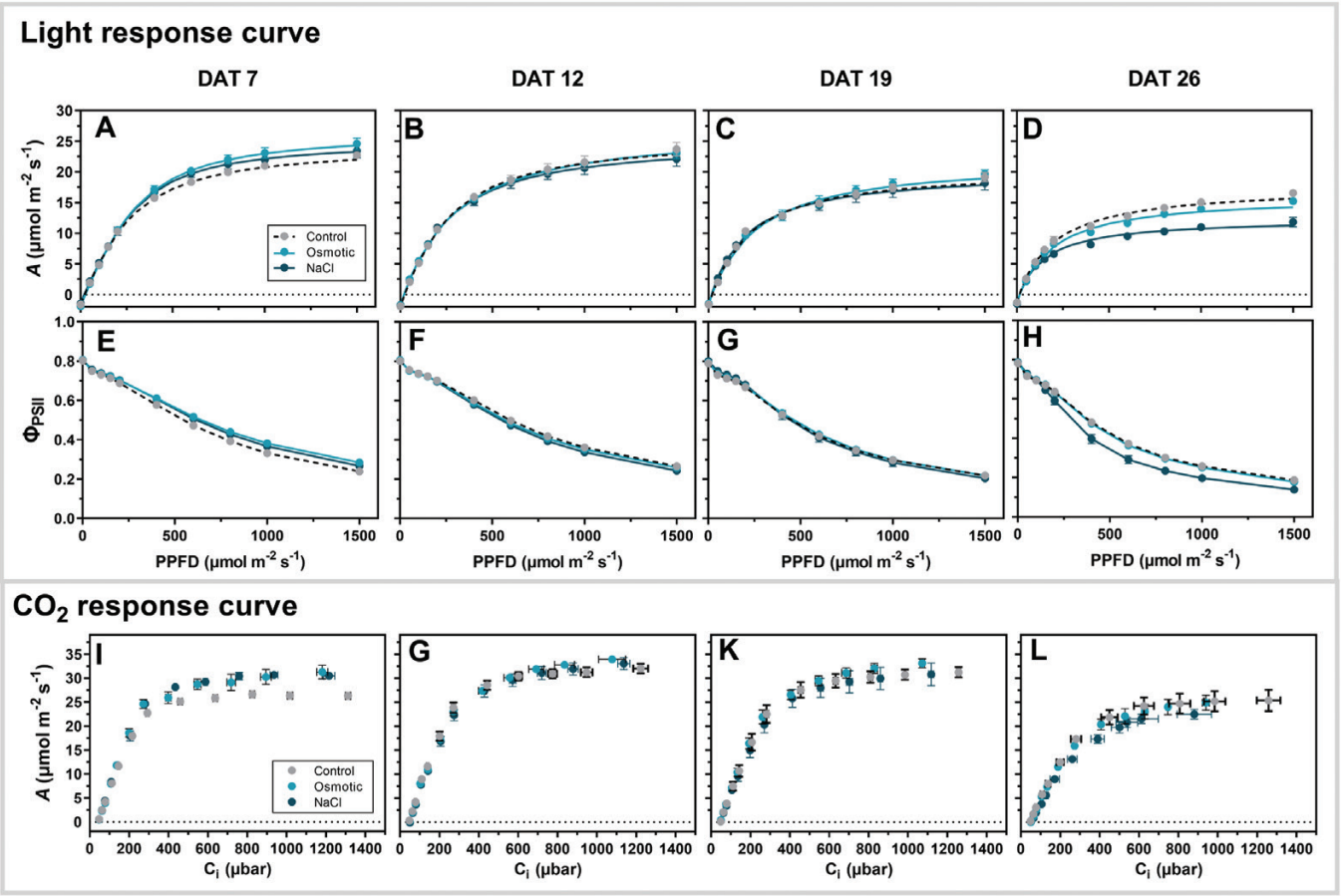

Fig. 1. Steady-state light and CO_2 response curves of leaf photosynthesis in the third true leaves of tomato plants, counting from the bottom of the plant. Responses of leaf net photosynthesis (*A*) (A–D) and photosystem II electron transport efficiency (Φ_{PSII}) (E–H) to incident PPFD, and responses of *A* to leaf internal CO_2 partial pressure (C_i) (I–L). Plants were subjected to three treatments: control (EC=2.3 dS m^{-1}), osmotic (EC≈12.6 dS m^{-1}, with concentrated macronutrients in the nutrient solution), and NaCl (EC≈12.8 dS m^{-1}, control solution with additional 100 mM NaCl). Measurements were conducted ±1 d from the date shown above the column (indicated as days after treatment started, DAT). Mean values ±SEM from four to five plants, grown in two separate experiments, are shown; SEM is visible only when larger than the data point symbol.

where g_{si} represents steady-state g_s under 50 μmol m^{-2} s^{-1} and g_{sf} represents steady-state g_s under 1500 μmol m^{-2} s^{-1}; λ represents an initial lag time (time after the increase in PPFD during which no change in g_s is observed); and k_i represents the time constant for an increase of g_s. k_i does not directly represent a time to reach a percentage of g_s, as this also depends on λ. Therefore, τ_i, which represents the time to reach 63% of the total g_s increase including λ, can be calculated as:

$$\tau_i = \lambda - k_i \times [\ln(-\ln(1 - e^{-1})) - 1] \quad (2)$$

After a step decrease in PPFD, the following exponential model was the best fit for stomatal closure in all data sets:

$$g_s = g_{si} + (g_{sf} - g_{si})e^{-t/\tau_d} \quad (3)$$

where τ_d represents the time to reach 63% of the total g_s decrease.

Growth and chemical analysis

Whole plants were dissected into leaves, stems, and roots. Then, the fresh weight of each organ, and the leaf number and leaf area, were determined. The components were then dried at 80°C for 3 d and their dry weights were measured. Dry leaf samples harvested at 19 DAT and 26 DAT were used to measure macronutrient concentrations (Eurofins Agroscience Services NL, Wageningen, The Netherlands), and leaves from three plants were analyzed as a pooled sample; samples harvested at 6 DAT and 12 DAT were not used, as they comprised too little material for this test.

Leaf chlorophyll concentration

Leaf discs (2 cm^2) punched from the third true leaves counted from the bottom of the plant (the same leaves as those used for photosynthesis measurements) were immersed in liquid nitrogen and then stored at –80°C. Leaf chlorophyll was extracted from frozen leaves with ice-cold 80% acetone. After centrifugation at 21 100 *g* for 5 min at 4 °C, the absorbance of the supernatant was measured at 470, 647, 664 and 750 nm wavelengths using a Varian Cary 4000 UV-Vis spectrophotometer (Agilent Technologies, Santa Clara, CA, USA), and the concentrations of chlorophyll *a*, chlorophyll *b*, and total carotenoids were calculated according to Porra *et al.* (1989) and Lichtenthaler (1987).

Statistical analysis

One-way ANOVA in randomized blocks (experiments as blocks) was performed to test the differences among the three treatments on a given

day after the start of treatment. The least significant difference test was used to assess differences between any two treatments at the P=0.05 level. Two-way ANOVA was used on the time-series data to test the interaction effect and main effects of treatments and days after the start of treatment. Regression analyses were performed to test for correlations between parameters during photosynthetic and stomatal dynamics. All analyses were performed using Genstat 20th edition (VSN International, Hemel Hempstead, UK).

Results

Plant growth, dry matter partitioning, and nutrient content

Plants grown in osmotic and NaCl solutions had a significantly smaller biomass than control plants (30–36% reduction of plant dry weight at 26 DAT), and there was no difference between the two stress treatments (Supplementary Fig. S3A). Similar patterns were observed for leaf area and biomass (Supplementary Table S2). Both stress treatments increased partitioning of dry mass to the roots and stems, and decreased partitioning to the leaves (Supplementary Fig. S3B). Compared with the NaCl treatment, the osmotic treatment increased partitioning of dry mass to the roots and decreased partitioning to the leaves (Supplementary Fig. S3B).

The leaf mineral concentrations of plants grown under osmotic stress differed from those of control plants by an increase in the concentrations of N and K of 12%, Mg of ~28%, and S of ~67%, and by a decrease in the concentration of Ca of ~21% (Supplementary Table S3). In NaCl-treated plants, the concentrations of Na and Cl strongly increased, and that of K decreased by 43–49%, compared with both control and osmotic treatments, while the concentrations of other minerals were similar to those in the control plants (Supplementary Table S3).

Leaf thickness and pigmentation

Initially, leaves of control plants were significantly thinner (larger specific leaf area) than those grown in the osmotic and NaCl treatments (at 6 DAT and 12 DAT; Supplementary Table S2). With time, leaves in all treatments became thicker, and the initial difference among treatments disappeared.

Total chlorophyll contents (Chl a+b) per unit leaf area increased throughout the development of the third leaf, with a tendency for the Chl a:b ratio to decrease (Supplementary Fig. S4, Supplementary Table S4). Leaves of plants in the osmotic and NaCl treatments initially displayed similarly enhanced Chl a+b (6 DAT in Supplementary Fig. S4), which was 50–60% higher than the control. With time, Chl a+b in the NaCl treatment declined compared with the osmotic treatment (Supplementary Fig. S4). At 26 DAT, Chl a+b in the osmotic treatment was 30–35% higher than in the other treatments. The Chl a:b ratio showed only small differences among treatments (Supplementary Table S4).

Steady-state photosynthesis

During the first 3 weeks, the A/PPFD response in the third leaf was not significantly different among treatments (Fig. 1A–C). A under higher C_i (>600 μbar) was increased in both stress treatments at 7 DAT compared with control (Fig. 1I), but this difference disappeared at 12 DAT and 19 DAT (Fig. 1G, K). At 26 DAT, light-saturated A was lowest in the NaCl treatment compared with both other treatments (Figs 1D, 2A), along with reduced V_{cmax} and photosystem II (PSII) electron transport efficiency (Φ_{PSII}) (Figs 1H, 1L, 2G). The most prominent difference between treatments was that of $\bar{g}_s$ (Fig. 2D, P_T<0.001). Both the osmotic and NaCl treatments decreased $\bar{g}_s$ compared with the control treatment, this decrease being 7–25% for the osmotic treatment and even larger (~50%) for the NaCl treatment at 26 DAT (Fig. 2D). No significant differences in α, R_{dark}, g_m, maximum PSII efficiency (F_v/F_m), and J_{1500} were found between treatments (Fig. 2). All parameters describing steady-state photosynthesis, except R_{dark}, changed as the leaf developed (P_D<0.001). For example, in the control treatment, A_{max}, $\bar{g}_s$, V_{cmax}, and J_{1500} decreased as the leaf developed (Fig. 2A, C, D, G, H), whereas g_m, F_v/F_m, and TPU peaked and then declined during leaf development (Fig. 2E, F, I). A expressed per unit chlorophyll (A_{chl}) was similarly reduced by the osmotic and NaCl treatments compared with the control treatment (Supplementary Fig. S5).

Photosynthetic induction

To examine photosynthetic properties under dynamic light conditions, gas exchange and chlorophyll fluorescence were measured under several light intensity step changes. At 6 DAT and 11 DAT, when leaves adapted to 50 μmol m^{-2} s^{-1} were suddenly exposed to 1500 μmol m^{-2} s^{-1}, no differences in A between treatments were observed (Fig. 3A, D). However, after a subsequent 30 min exposure to low light followed by reillumination with high light intensity, transient A was decreased by 7–9% in both stress treatments (Fig. 3A, D). At 19 DAT, leaves grown in both stress treatments showed decreased A (12–25%) during the first 10 min of photosynthetic induction (Fig. 3G). At 25 DAT, leaves grown in NaCl had the lowest A during both induction phases, compared with both other treatments (Figs 3J, 4F). At that moment, leaves grown in NaCl started to show significantly decreased Φ_{PSII} kinetics compared with the control and osmotic treatments, whereas non-photochemical fluorescence quenching kinetics were unaffected (Supplementary Fig. S6L, P). The reduction of transient Φ_{PSII} in the NaCl treatment was due to a lower photochemical fluorescence quenching rather than a change in F_v'/F_m' (Supplementary Fig. S6D, H). Average A ($\bar{A}_{300}$), IS_{60}, t_{50}, and t_{90} were characterized for both induction phases. The only treatment effect was seen at 19 DAT, with a higher IS_{60} and $\bar{A}_{300}$ in the control treatment compared with both stress treatments (Fig. 4A, B, G, H). t_{50} tended to increase, and t_{90} to

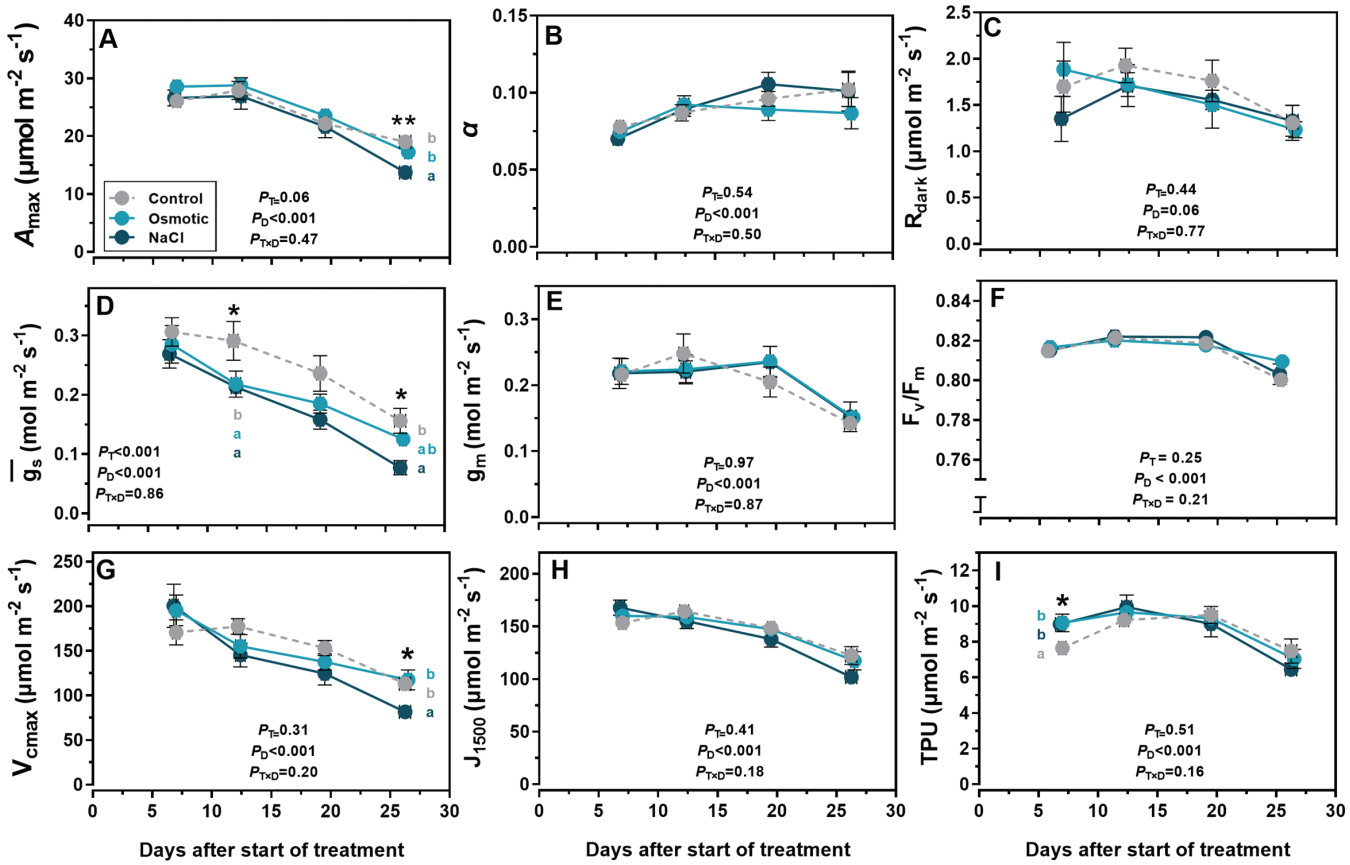

Fig. 2. Effects of NaCl and leaf age on traits characterizing steady-state photosynthesis in third true leaves of tomato plants, counting from the bottom of the plant. (A) Maximum net photosynthetic rate (A_{max}); (B) apparent quantum yield (α); (C) dark respiration rate (R_{dark}); (D) average stomatal conductance during light response curves of leaf photosynthesis ($\bar{g}_s$); (E) mesophyll conductance (g_m); (F) maximum quantum efficiency of photosystem II photochemistry (F_v/F_m); (G) maximum carboxylation rate (V_{cmax}); (H) electron transport rate at 1500 μmol m^{-2} s^{-1} PPFD (J_{1500}); (I) triose phosphate use (TPU). Plants were subjected to three treatments: control (EC=2.3 dS m^{-1}), Osmotic (EC≈12.6 dS m^{-1}, with concentrated macronutrients in the nutrient solution), and NaCl (EC≈12.8 dS m^{-1}, control solution with additional 100 mM NaCl). Mean values ±SEM from four to five plants, grown in two separate experiments, are shown; SEM is visible only when larger than the data point symbol. Asterisks indicate significant differences between treatments on the given day after treatment (*P<0.05, **P<0.01) and different letters show statistically significant differences between treatments at P=0.05. Two-way ANOVA was performed for each parameter, and the P-value of the main effect of treatment (P_T) and days after start of treatment (P_D), as well as the interaction effect of the two factors ($P_{T×D}$), is shown.

decrease, over time in both stress treatments, relative to the control treatment (P_T<0.001; Fig. 4D, I). In addition, t_{50} during the second induction phase was strongly increased (>150%) in both stress treatments (Fig. 4I), along with a relatively higher stomatal limitation during the first 10 min of induction, compared with control leaves (Supplementary Fig. S7I–L). As the leaf developed, $\bar{A}_{300}$ declined (Fig. 4A, G). During the first induction phase, t_{50} and t_{90} increased with leaf development (P_D<0.01, Fig. 4C, D), as did stomatal and non-stomatal limitations (Supplementary Fig. S7A–H). During the second induction phase, IS_{60} and t_{50} were constant with leaf maturation (P_D>0.05, Fig. 4H, I).

Dynamic stomatal behavior

Increasing light intensity from 50 μmol m^{-2} s^{-1} to 1500 μmol m^{-2} s^{-1} and then decreasing it to 50 μmol m^{-2} s^{-1} induced strong stomatal responses (Fig. 3). The increase in g_s followed a sigmoidal pattern, whereas the decrease in g_s followed an exponential pattern. g_s in both stress treatments reached a steady state after 60 min of high PPFD, whereas g_s in control leaves did not (Fig. 3). The 30 min exposure to low PPFD after high PPFD was often insufficient for complete, steady-state stomatal closure. However, g_s at the end of 30 min of low PPFD was close to or even smaller than g_s at the beginning of the measurements (e.g. at 6 DAT and 11 DAT; Fig. 3B, E).

Steady-state g_s at the initial PPFD (g_{si}) and final g_s after 60 min exposure to high PPFD (g_{sf}) were higher in the control treatment than in both stress treatments (Fig. 5A, B), although the effects on g_{si} were small and significant only at 19 DAT. Leaves of plants grown in the osmotic and NaCl treatments showed similar g_{si} and g_{sf} before 19 DAT, whereas at 25 DAT, g_{sf} in the NaCl treatment was ~40% lower than that in the osmotic treatment (Fig. 5A, B). The initial lag time in the g_s

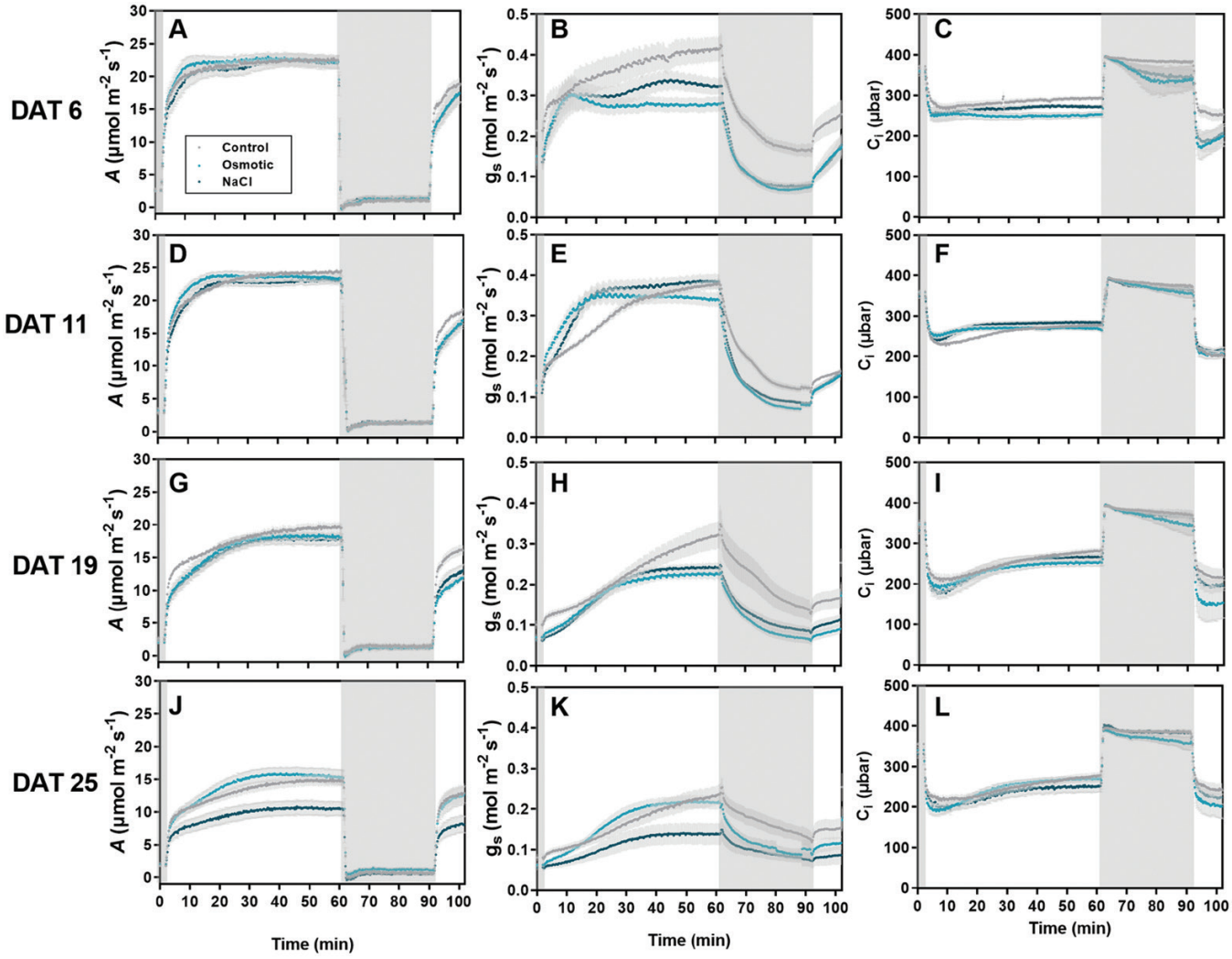

Fig. 3. Time courses of leaf net photosynthetic rate (*A*) (A, D, G, J), stomatal conductance (g_s) (B, E, H, K), and leaf internal CO_2 partial pressure (C_i) (C, F, I, L) when the third true leaf of tomato plants (counting from the bottom of the plant) was subjected to changes in irradiance. Low light (50 µmol m^{-2} s^{-1}) adapted leaves were first exposed to a step increase in light intensity (1500 µmol m^{-2} s^{-1}); then, after a 30 min exposure to low light (indicated by the grey box), leaves were reilluminated with high light. Plants were subjected to three treatments: control (EC=2.3 dS m^{-1}), osmotic (EC≈12.6 dS m^{-1}, with concentrated macronutrients in the nutrient solution), and NaCl (EC≈12.8 dS m^{-1}, control solution with additional 100 mM NaCl). Measurements were conducted ±1 d from the date shown in each row (indicated as days after treatment started, DAT). Mean values ± SEM from 7–10 plants, grown in three separate experiments, are shown.

increase (λ) went up strongly in all cases as the leaf developed (Supplementary Fig. S8A). Time constants of g_s increase, either including or excluding λ (k_i and τ_i, respectively), and of g_s decrease (τ_d), were larger in the control treatment compared with both stress treatments, and were similar in the osmotic and NaCl treatments (Fig. 5C, D; Supplementary Fig. S8B). Finally, time constants in all treatments increased as the leaves developed (Fig. 5C, D; Supplementary Fig. S8B).

Across treatments, there was a consistent threshold-type relationship between g_{si} and photosynthetic induction rate (t_{50} and t_{90}): at g_{si} <0.13 mol m^{-2} s^{-1}, g_{si} was significantly negatively correlated with t_{50} (Fig. 6A); at g_{si} <0.22 mol m^{-2} s^{-1}, g_{si} was significantly negatively correlated with t_{90} (Fig. 6B). At larger g_{si}, photosynthetic induction rate was not affected by g_{si}. The time constant for g_s increase (τ_i) was significantly correlated with t_{90} but not t_{50} (Fig. 6C, D).

Discussion

Dynamic stomatal behavior is affected by NaCl stress and leaf age

Osmotic effects of NaCl stress induce rapid stomatal responses to changes in light intensity

Stomata regulate CO_2 influx into and water vapor efflux out of the leaf. In nature, due to slow responses of stomata to highly

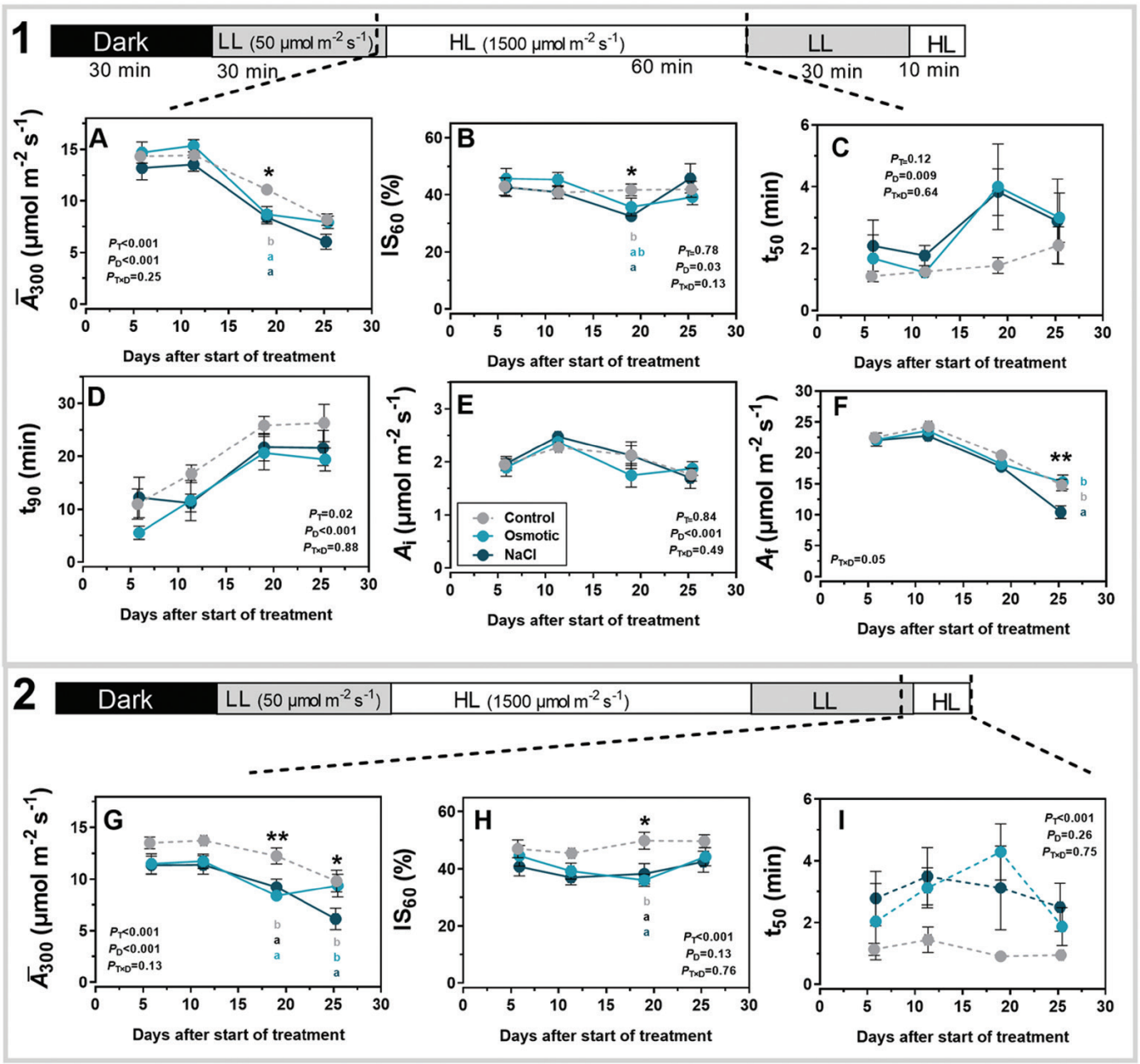

Fig. 4. Effects of NaCl and leaf age on traits characterizing the rate of photosynthetic induction in the third true leaves of tomato plants, counting from the bottom of the plant. (A, G) Average A during the first 300 s of induction ($\bar{A}_{300}$); (B, H) photosynthetic induction state 60 s after illumination (IS_{60}); (C, I) time required to reach 50% of full photosynthetic induction (t_{50}); (D) time required to reach 90% of full photosynthetic induction (t_{90}); (E, F) steady-state A at (E) 50 µmol m^{-2} s^{-1} PPFD (A_i) and (F) 1500 µmol m^{-2} s^{-1} PPFD (A_f). Two scenarios of step increase in irradiance (indicated with 1 and 2) under a period of dynamic light intensity are shown: in scenario 1, low light (50 µmol m^{-2} s^{-1}) adapted leaves were first exposed to a step increase in light intensity (1500 µmol m^{-2} s^{-1}); in scenario 2, after a 30 min exposure to low light, leaves were reilluminated with high light. Plants were subjected to three treatments: control (EC=2.3 dS m^{-1}), osmotic (EC≈12.6 dS m^{-1}, with concentrated macronutrients in the nutrient solution), and NaCl (EC≈12.8 dS m^{-1}, control solution with additional 100 mM NaCl). Mean values ±SEM from 7–10 plants, grown in three separate experiments, are shown, and SEM is visible only when larger than the data point symbol. Asterisks indicate significant differences between treatments on the given day after treatment (*P<0.05, **P<0.01) and different letters show statistically significant differences between treatments at P=0.05. Two-way ANOVA was performed for each parameter; the P-value of the main effect of treatment (P_T) and days after start of treatment (P_D), as well as the interaction effect of two factors ($P_{T\times D}$), is shown.

variable light intensity, g_s does often not reach a steady state (Lawson and Blatt, 2014). NaCl stress decreased steady-state g_s at low and high light intensity (Fig. 5A, B), and induced faster increases and decreases in g_s under FL (τ_i and τ_d; Fig. 5C, D). These more rapid g_s responses were consistently observed throughout the 4 weeks of NaCl stress, and were mainly caused

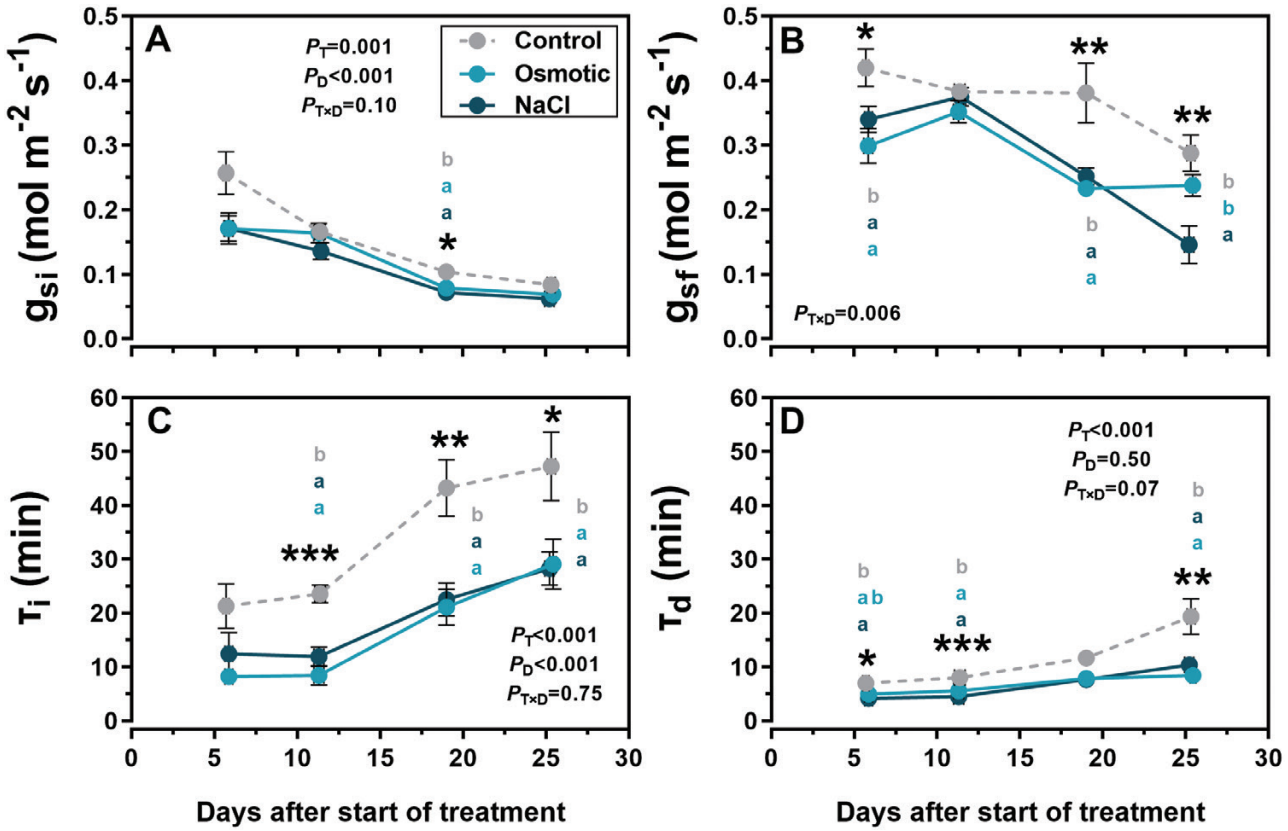

Fig. 5. Effects of NaCl and leaf age on traits characterizing dynamic stomatal behavior in third true leaves of tomato plants, counting from the bottom of the plant. (A) Steady-state g_s under 50 μ mol m^{-2} s^{-1} (g_{si}); (B) steady-state g_s under 1500 μmol m^{-2} s^{-1} (g_{sf}); (C) time to reach 63% of the total g_s increase (including the initial lag time) (τ_i); (D) time to reach 63% of the total g_s decrease from high to low PPFD (τ_d). Plants were subjected to three treatments: control (EC=2.3 dS m^{-1}), osmotic (EC≈12.6 dS m^{-1}, with concentrated macronutrients in the nutrient solution), and NaCl (EC≈12.8 dS m^{-1}, control solution with additional 100 mM NaCl). Mean values ±SEM from 7–10 plants, grown in three separate experiments, are shown, and SEM is visible only when larger than the data point symbol. Asterisks indicate significant differences between treatments on the given day after treatment (*P<0.05, **P<0.01, ***P<0.001) and different letters show statistically significant differences between treatments at P=0.05. Two-way ANOVA was performed for each parameter and the P-value of the main effect of treatment (P_T) and days after start of treatment (P_D), as well as the interaction effect of the two factors ($P_{T\times D}$), is shown.

by the osmotic effect, as both stress treatments showed similar values for τ_i and τ_d (Fig. 5C, D). Faster g_s responses under FL were previously observed in water-stressed plants (Lawson and Blatt, 2014; Qu *et al.*, 2016) and at high vapor pressure deficit (Tinoco-Ojanguren and Pearcy, 1993; Kaiser *et al.*, 2017). Studies on the genotypic variation of these traits do not suggest a general relationship between g_s amplitude (g_{sf}–g_{si}) and time constants of stomatal movement (McAusland *et al.*, 2016; Xiong *et al.*, 2018); a faster g_s response under FL, independent of g_s amplitude, could thus be a strategy for tighter stomatal regulation to prevent unnecessary evaporative loss under osmotic stress (Papanatsiou *et al.*, 2019; Kimura *et al.*, 2020; Yamori *et al.*, 2020).

The fast speed of the g_s response to FL under osmotic stress meant an increased ability of guard cells to perceive environmental changes, transduce the signal, and induce changes in cell turgor (Lawson and Blatt, 2014; Lawson and Vialet-Chabrand, 2019; Nunes *et al.*, 2020), possibly due to changes in stomatal morphology and physiology as affected by hydraulic and hormonal signals. Although we did not measure stomatal size, a study from our group reported that stomata were ~18% smaller under NaCl stress in tomato (Zhang *et al.*, 2020). Generally, smaller stomata have a greater membrane surface area-to-volume ratio (Drake *et al.*, 2013), which may induce faster movement, although this differs among plant species (Zhang *et al.*, 2019; Sakoda *et al.*, 2020). Additionally, osmotic stress could alter the density and activity of transport proteins across the guard cell plasma membrane (Luan, 2002), in turn inducing faster stomatal movement. Further, we assume that treatment-induced differences in leaf K concentration (Supplementary Table S3) did not affect dynamic stomatal behavior, as a small increase in K concentration in the osmotic treatment and a large decrease in K concentration in the NaCl treatment were associated with to similar speeds of stomatal opening and closure in the two treatments (Fig. 5C, D). The different hypotheses for faster stomatal movement under osmotic stress

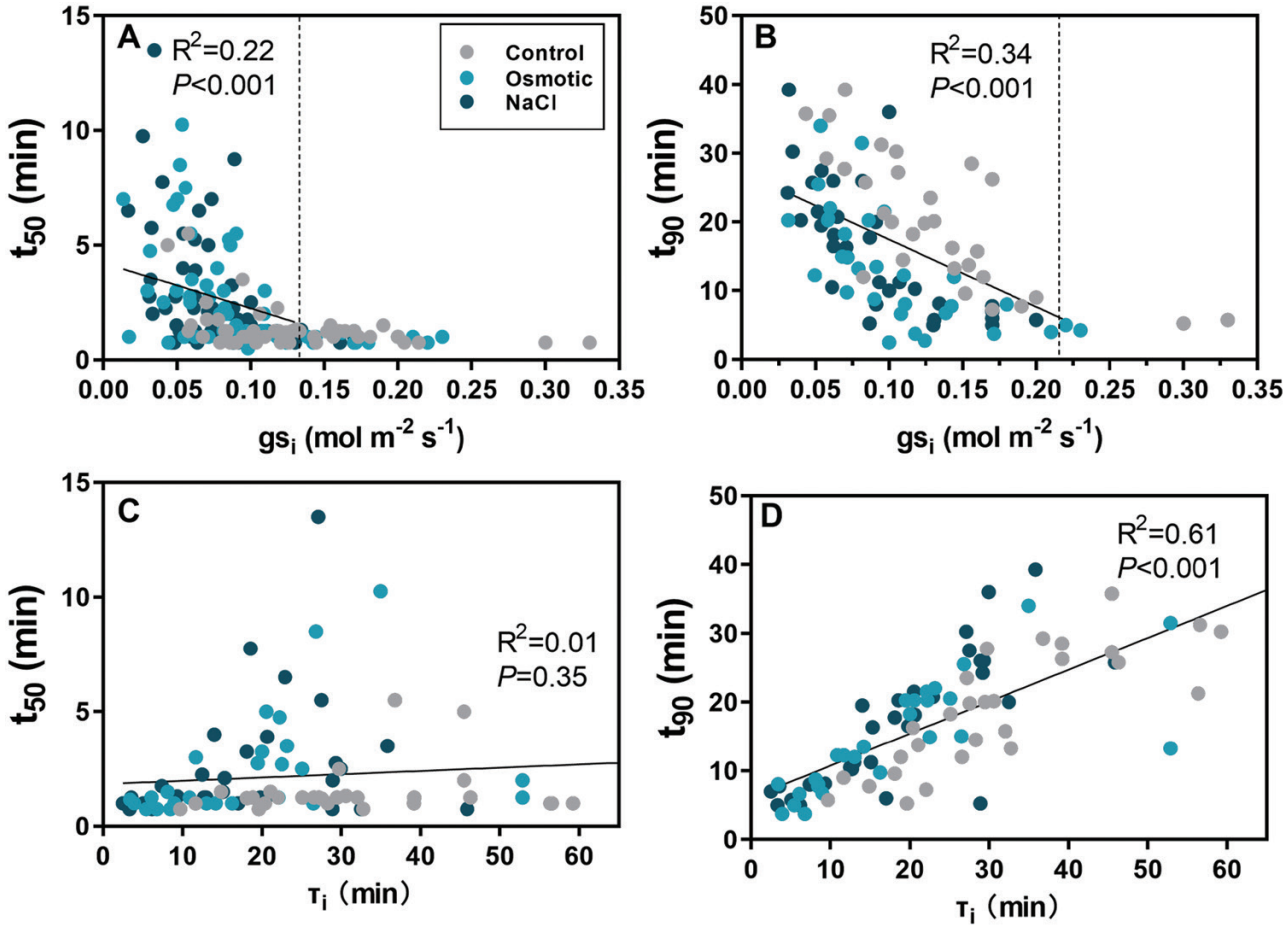

Fig. 6. Relationships between stomatal conductance, stomatal movement, and rate of photosynthetic induction. Individual measures, regression lines, correlation coefficient (R^2), and *P*-value for (A) t_{50} versus g_{si}, (B) t_{90} versus g_{si}, (C) t_{50} versus τ_i, and (D) t_{90} versus τ_i. t_{50} and t_{90}, time required to reach 50% and 90% of full photosynthetic induction, respectively; g_{si}, steady-state g_s under 50 μmol m^{-2} s^{-1}; τ_i, time to reach 63% of the total g_s increase (including the initial lag time). Data were derived from the first induction phase, as shown in Fig. 4.

require further study; one approach could be to integrate the molecular, biophysical, and kinetic characteristics of guard cells (e.g. ion transport, malate metabolism, and H^+ and Ca^{2+} buffering; see Lawson and Matthews, 2020) under osmotic stress and connect this information to stomatal kinetics and behavior under dynamic light.

In older leaves, the stomatal response to dynamic light conditions becomes sluggish

Steady-state g_s, which depends on stomatal density and guard cell size, is constrained by leaf development (Murchie *et al.*, 2005; Wu *et al.*, 2014). To our knowledge, the effects of leaf age on stomatal movement under FL have not yet been studied. Our results showed that as leaves aged, steady-state (Fig. 5A, B) and transient g_s responses to light were damped, the latter being shown by an increased g_s lag time after a step increase in PPFD (λ; Supplementary Fig. S8A) as well as increases in τ_i and τ_d (Fig. 5C, D) throughout leaf maturation. This change in the rapidity of the stomatal response to both increases and decreases in light intensity may be ascribed to developmentally driven changes in stomatal size or ion channels in guard cells (Pantin *et al.*, 2012; Durand *et al.*, 2019). Characterization of stomatal kinetics at different leaf developmental stages in mutants and transformant lines (Lawson and Blatt, 2014; Lawson and Matthews, 2020) and input from g_s kinetic models (e.g. OnGuard models; Y. Wang *et al.*, 2017) may provide future insights into the drivers of g_s throughout leaf development.

Dynamic photosynthesis is affected by NaCl stress and leaf age

In nature, leaf photosynthesis occurs largely under FL, and time-integrated A depends on both steady-state A and the rapidity of the response of A to changes in PPFD. During photosynthetic induction, steady-state photosynthesis is largely determined by photosynthetic capacity. The rapidity of the response of A to FL is usually quantified as the rate of photosynthetic induction after low-to-high PPFD transitions. We found

that the averaged photosynthesis rate ($\bar{A}_{300}$) generally declined with leaf age (Fig. 4A, G), and both osmotic stress (at 19 DAT) and ionic stress (at 26 DAT) added to this reduction in a time-dependent manner (Fig. 4A, G).

Photosynthetic capacity drops during leaf development, and the ionic effect accelerates this process

Leaves situated close to the bottom of a dense canopy have lower photosynthetic capacity than leaves at the top, which is caused by progressive shading rather than leaf age (Hikosaka, 1996; Trouwborst *et al.*, 2015; Collison *et al.*, 2020). In our study, full light exposure of the third leaf was ensured throughout the experiment, to rule out any shade effects on the leaf of interest. We found that photosynthetic capacity decreased as the leaf aged, concomitantly with a gradual reduction in Rubisco carboxylation capacity (V_{cmax}; Fig. 2G) and electron transport rates under high light (J_{1500}; Fig. 2H), and despite increasing chlorophyll contents (Supplementary Fig. S4). The ionic effect of NaCl stress is known to accelerate senescence in mature leaves (Munns and Tester, 2008), and this was also observed in older leaves (at 26 DAT): A was largely down-regulated by the ionic effect (in the NaCl treatment but not the osmotic stress treatment). This was caused by impaired electron transport efficiency (Supplementary Fig. S6L), down-regulation of carboxylation capacity (Fig. 2G), and a further reduction in g_s (Fig. 2D). At the whole-plant level, no ionic effect was detectable, as biomass was similarly reduced in both stress treatments (Supplementary Fig. S3A). Notably, judging from A/PPFD curves (Fig. 1D), almost no differences in A were observed under the growth light intensity (200 μmol m^{-2} s^{-1}) among all treatments. These results lead us to assume that the strong reduction in biomass under both stress treatments was mainly due to a smaller leaf area (light interception area) rather than a reduction in A per unit leaf area, and that the reduction in leaf area expansion was mainly due to osmotic effects, in line with Munns and Tester (2008). If plants were to grow under more natural, occasionally very high (1000–2000 μmol m^{-2} s^{-1}) light intensities, we assume that the ionic effect on leaf photosynthesis would reduce plant growth additionally to the osmotic effect seen in our experiment.

Compared with the ionic effect, the osmotic effect hardly reduced photosynthetic capacity (Fig. 1A–D), even though g_s was reduced under this treatment (Fig. 2D). On a chlorophyll basis, however, the lower A_{chl} in both stress treatments (Supplementary Fig. S5) suggested a reduction in photosynthetic efficiency per unit chlorophyll that was caused by osmotic stress. Most likely, smaller and thicker leaves, as well as increased chloroplast density per unit leaf area (Supplementary Fig. S4, Supplementary Table S4; Munns and Tester, 2008; Niinemets *et al.*, 2009; Wungrampha *et al.*, 2018), compensated for this reduction in A_{chl}, resulting in similar to higher photosynthetic capacity compared with non-stressed leaves (e.g. at 7 DAT, A was increased in the osmotic and NaCl treatments under saturating CO_2 partial pressures compared with the control treatment; Fig. 1I).

The rate of photosynthetic induction under NaCl stress is affected by osmotic stress and leaf age, rather than by ionic effects

NaCl stress affected photosynthetic induction mainly through osmotic effects (Fig. 4). Consistent with previous results (Zhang *et al.*, 2018), osmotic stress tended to decrease photosynthetic induction (increased IS_{60} and t_{50}; Fig. 4H, I, P_T<0.001). However, we also observed that osmotic stress increased photosynthetic induction during the late phase of induction, as suggested by a decreased t_{90} (Fig. 4D, P_T=0.02). Often, a threshold value for g_{si} effects on the rate of photosynthetic induction was found (Valladares *et al.*, 1997; Allen and Pearcy, 2000; Kaiser et al., 2016, 2020). A study comparing tomato cv. Rheinlands Ruhm with its abscisic acid-deficient *flacca* mutant showed that a g_{si} <0.2 mol m^{-2} s^{-1} was negatively correlated with t_{50}, and g_{si} <0.4 mol m^{-2} s^{-1} was negatively correlated with t_{90} (Kaiser *et al.*, 2020). We observed a different threshold g_{si} value for tomato cv. Moneymaker across treatments, namely g_{si} <0.13 mol m^{-2} s^{-1} for t_{50} and g_{si} <0.22 mol m^{-2} s^{-1} for t_{90} (Fig. 6A, B). However, photosynthetic induction was determined not only by g_{si} but also by how fast stomata opened after increases in light intensity, as suggested by a significant correlation between τ_i and t_{90} (Fig. 6D). Under osmotic stress, g_s showed an immediate and more rapid increase, which lowered t_{90} (Fig. 4D). Rapid g_s kinetics in transitions from low to high light have been hypothesized to maximize A, as steady-state values under the new conditions can be rapidly achieved (Kimura *et al.*, 2020). However, under osmotic stress, stomata also closed more quickly under low light, reducing the photosynthetic induction rate when the light intensity increased again (second induction, Fig. 4). This is similar to the effects of drought stress on g_s kinetics (see Figs 3F and 4 in Lawson and Blatt, 2014). Thus, g_s kinetics are, together with steady-state g_s (at low and high light intensity), crucial for photosynthetic performance under fluctuating light.

The effects of leaf age on dynamic photosynthesis traits have so far received little attention. To our knowledge, only one study (Urban *et al.* 2008) compared photosynthetic induction between young and mature leaves, in poplar; however, in that study, young and mature leaves were likely acclimated to very different light intensities, so leaf age was not the only differentiating factor. In our study, we ensured that leaves were exposed to the same light intensity throughout development. Photosynthetic induction rate decreased with increasing leaf age (increased t_{50} and t_{90}; Fig. 4C, D), caused by increases in both stomatal and non-stomatal limitations (Supplementary Fig. S7). Non-stomatal limitation is caused by slow activation of electron transport and Calvin–Benson cycle enzymes (especially Rubisco; Sakoda *et al.*, 2021), and possibly changes in mesophyll conductance (Liu *et al.*, 2022). After 19 DAT, a persistent non-stomatal limitation after 10 min during the first

induction meant that Rubisco limitation increased as the leaf developed (Supplementary Fig. S7E–H). In addition, the decrease in g_{si} and increase in τ_i as the leaf developed (Fig. 5) may have increased transient stomatal limitations (Supplementary Fig. S7).

Perspectives on methods to disentangle the osmotic and ionic effects of salt stress

The search for the optimal medium for imposing osmotic stress has been ongoing for decades. Carbohydrates (e.g. mannitol and sorbitol), high-molecular-weight polyethylene glycol (PEG), and concentrated mixed salts have been recommended, but none of the existing methods is perfect. First, PEG is often used to induce osmotic stress in studies aimed at disentangling the osmotic and ionic effects of salt stress (e.g. Castillo *et al.*,2007; Lan *et al.*, 2020). However, as PEG can enter the roots and reduce hydraulic conductivity, experiments must be limited to a short period of time; for this reason, we decided against using PEG in our experiments. Concentrated macronutrients are a viable alternative, as their rate of uptake is tightly regulated by transporters, and they do not support bacterial growth as carbohydrates often do (Munns, 2011). However, the toxicity of specific ions (e.g. ammonium), or their imbalance due to precipitation, requires careful mixing of macronutrient solutions. Further, while it is often assumed that the salt causing stress is NaCl, many different categories of saline soil exist, arising from different mineral compositions and different types of salinization, all affecting plant responses through osmotic pressure or specific ion concentrations (Rengasamy, 2010*b*; Ludwiczak *et al.*, 2021). On irrigated farmland in particular, the recent trend of irrigating crops using recycled water may lead to high concentrations of macronutrients other than Na and Cl (Rengasamy, 2010*b*). Our study may provide insights on how salts other than NaCl affect photosynthesis and stomatal kinetics under dynamic light.

Conclusions

Our study describes how NaCl stress, along with leaf age, regulates stomatal behavior and carbon assimilation in tomato leaves under dynamic light intensities (summarized in Table 1), which is highly relevant for field- and greenhouse-grown plants. Results show that (i) stomatal and photosynthetic performance under FL was strongly affected by all three of osmotic effects, ionic effects, and leaf ageing; (ii) osmotic effects of NaCl occurred first, and induced a reduction in g_s, along with rapid stomatal responses to changes in light intensity, which affected photosynthetic induction but not steady-state photosynthesis and photosynthetic capacity; (iii) ionic effects of NaCl on photosynthesis occurred after 26 d of NaCl exposure and were visible as a reduction in both photosynthetic capacity and g_s, but effects on photosynthetic induction rate and stomatal response rate were barely observed; and (iv) leaf photosynthetic capacity, photosynthetic induction rate, and stomatal response rate declined with increasing leaf age.

Table 1. Direction of response in dynamic stomatal and photosynthetic traits to osmotic and ionic effects

Parameter	Osmotic effect	Ionic effect	Leaf age
g_{si}	↓	–	↓
g_{sf}	↓	↓	↓
Rate of g_s increase	↑	–	↓
Rate of g_s decrease	↑	–	↓
A_{max}	–	↓	↓
Induction rate	–/↓/↑	–	↓
Induction gain[a]	–/↓	↓	↓

Arrows indicate the direction of the response of the trait (↑= increase, ↓ = decrease); a dash (–) represents no change.

[a] Accumulated photosynthetic rate during photosynthetic induction.

Supplementary data

The following supplementary data are available at *JXB* online.

Table S1. Characteristics of nutrient solution per treatment.

Table S2. Growth traits of whole plants.

Table S3. Leaf mineral concentrations.

Table S4. Leaf pigment concentrations.

Fig. S1. Tomato plant grown in a container with 7.6 litres of nutrient solution.

Fig. S2. Spectrum of growth light.

Fig. S3. Plant dry mass and its partitioning to leaves, stems, and roots.

Fig. S4. Chlorophyll concentration in the third true leaves, counting from the bottom of the plant.

Fig. S5. Steady-state light response curves of leaf net photosynthesis, expressed per unit chlorophyll.

Fig. S6. Chlorophyll fluorescence parameters during photosynthetic induction.

Fig. S7. Time courses of transient stomatal and non-stomatal limitations.

Fig. S8. Changes in traits characterizing dynamic stomatal opening.

Acknowledgements

We thank David Brink, Gerrit Stunnenberg, Taede Stoker, Geurt Versteeg, and Sean Geurts for their technical support with climate chamber experiments; Dr Sander van Delden and Ms Xiaojing Zhang for providing instructions on the salt-stress setup; Dr Ep Heuvelink for guidance on the statistical analysis; and Ms Xuguang Sun for help with pigment measurements.

Author contributions

All authors conceived and designed the research; YZ performed all the experiments; YZ and EK wrote the manuscript; all authors read and edited the manuscript.

Conflict of interest

The authors declare no conflicts of interest.

Funding

The authors gratefully acknowledge financial support from the National Natural Science Foundation of China (no. 31872955), the Agricultural Science and Technology Innovation Program (ASTIP), the Central Public-interest Scientific Institution Basal Research Fund (no. BSRF202107, BSRF201911), and the China Scholarship Council.

Data availability

All data supporting the findings of this study are available within the paper and within its supplementary materials published online.

References

Allen MT, Pearcy RW. 2000. Stomatal versus biochemical limitations to dynamic photosynthetic performance in four tropical rainforest shrub species. Oecologia **122**, 479–486.

Cannell MGR, Thornley JHM. 1998. Temperature and CO_2 responses of leaf and canopy photosynthesis: a clarification using the non-rectangular hyperbola model of photosynthesis. Annals of Botany **82**, 883–892.

Castillo E, Tuong TP, Ismail AM, Inubushi K. 2007. Response to salinity in rice: comparative effects of osmotic and ionic stresses. Plant Production Science **10**, 159–170.

Chaves MM, Costa JM, Saibo NJ. 2011. Recent advances in photosynthesis under drought and salinity. In: Turkan I, ed. Plant responses to drought and salinity stress: developments in a post-genomic era. Advances in Botanical Research Vol. **57**. London: Elsevier, 49–104.

Collison RF, Raven EC, Pignon CP, Long SP. 2020. Light, not age, underlies the maladaptation of maize and miscanthus photosynthesis to self-shading. Frontiers in Plant Science **11**, 783.

Drake PL, Froend RH, Franks PJ. 2013. Smaller, faster stomata: scaling of stomatal size, rate of response, and stomatal conductance. Journal of Experimental Botany **64**, 495–505.

Durand M, Brendel O, Bure C, Le Thiec D. 2019. Altered stomatal dynamics induced by changes in irradiance and vapour-pressure deficit under drought: impacts on the whole-plant transpiration efficiency of poplar genotypes. New Phytologist **222**, 1789–1802.

FAO/ITPS. 2015. Status of the World's Soil Resources (SWSR) – Main Report. Rome: FAO.

Faralli M, Cockram J, Ober E, Wall S, Galle A, Van Rie J, Raines C, Lawson T. 2019. Genotypic, developmental and environmental effects on the rapidity of *gs* in wheat: impacts on carbon gain and water-use efficiency. Frontiers in Plant Science **10**, 492.

Ghorbani A, Razavi SM, Ghasemi Omran VO, Pirdashti H. 2018. *Piriformospora indica* inoculation alleviates the adverse effect of NaCl stress on growth, gas exchange and chlorophyll fluorescence in tomato (*Solanum lycopersicum* L.). Plant Biology **20**, 729–736.

Harley PC, Loreto F, di Marco G, Sharkey TD. 1992. Theoretical considerations when estimating the mesophyll conductance to CO_2 flux by analysis of the response of photosynthesis to CO_2. Plant Physiology **98**, 1429–1436.

Heuvelink E. 2018. Tomatoes. Wallingford: CABI.

Hikosaka K. 1996. Effects of leaf age, nitrogen nutrition and photon flux density on the organization of the photosynthetic apparatus in leaves of a vine (*Ipomoea tricolor* Cav.) grown horizontally to avoid mutual shading of leaves. Planta **198**, 144–150.

Kaiser E, Kromdijk J, Harbinson J, Heuvelink E, Marcelis LF. 2017. Photosynthetic induction and its diffusional, carboxylation and electron transport processes as affected by CO_2 partial pressure, temperature, air humidity and blue irradiance. Annals of Botany **119**, 191–205.

Kaiser E, Morales A, Harbinson J, Heuvelink E, Marcelis LFM. 2020. High stomatal conductance in the tomato *flacca* mutant allows for faster photosynthetic induction. Frontiers in Plant Science **11**, 1317.

Kaiser E, Morales A, Harbinson J, Heuvelink E, Prinzenberg AE, Marcelis LF. 2016. Metabolic and diffusional limitations of photosynthesis in fluctuating irradiance in *Arabidopsis thaliana*. Scientific Reports **6**, 31252.

Kimura H, Hashimoto-Sugimoto M, Iba K, Terashima I, Yamori W. 2020. Improved stomatal opening enhances photosynthetic rate and biomass production in fluctuating light. Journal of Experimental Botany **71**, 2339–2350.

Lan C-Y, Lin K-H, Chen C-L, Huang W-D, Chen C-C. 2020. Comparisons of chlorophyll fluorescence and physiological characteristics of wheat seedlings influenced by iso-osmotic stresses from polyethylene glycol and sodium chloride. Agronomy **10**, 325.

Lawson T, Blatt MR. 2014. Stomatal size, speed, and responsiveness impact on photosynthesis and water use efficiency. Plant Physiology **164**, 1556–1570.

Lawson T, Matthews J. 2020. Guard cell metabolism and stomatal function. Annual Review of Plant Biology **71**, 273–302.

Lawson T, Vialet-Chabrand S. 2019. Speedy stomata, photosynthesis and plant water use efficiency. New Phytologist **221**, 93–98.

Lichtenthaler HK. 1987. Chlorophylls and carotenoids: pigments of photosynthetic biomembranes. Methods in Enzymology **148**, 350–382.

Liu T, Barbour MM, Yu D, Rao S, Song X. 2022. Mesophyll conductance exerts a significant limitation on photosynthesis during light induction. New Phytologist **233**, 360–372.

Loriaux SD, Avenson TJ, Welles JM, McDermitt DK, Eckles RD, Riensche B, Genty B. 2013. Closing in on maximum yield of chlorophyll fluorescence using a single multiphase flash of sub-saturating intensity. Plant, Cell & Environment **36**, 1755–1770.

Luan S. 2002. Signalling drought in guard cells. Plant, Cell & Environment **25**, 229–237.

Ludwiczak A, Osiak M, Cardenas-Perez S, Lubinska-Mielinska S, Piernik A. 2021. Osmotic stress or ionic composition: which affects the early growth of crop species more? Agronomy **11**, 435.

McAusland L, Vialet-Chabrand S, Davey P, Baker NR, Brendel O, Lawson T. 2016. Effects of kinetics of light-induced stomatal responses on photosynthesis and water-use efficiency. New Phytologist **211**, 1209–1220.

Morales A, Kaiser E, Yin X, Harbinson J, Molenaar J, Driever SM, Struik PC. 2018. Dynamic modelling of limitations on improving leaf CO_2 assimilation under fluctuating irradiance. Plant, Cell & Environment **41**, 589–604.

Munns R. 2011. Plant adaptations to salt and water stress: differences and commonalities. Advances in Botanical Research **57**, 1–32.

Munns R, Tester M. 2008. Mechanisms of salinity tolerance. Annual Review of Plant Biology **59**, 651–681.

Murchie EH, Hubbart S, Peng S, Horton P. 2005. Acclimation of photosynthesis to high irradiance in rice: gene expression and interactions with leaf development. Journal of Experimental Botany **56**, 449–460.

Niinemets U, Diaz-Espejo A, Flexas J, Galmes J, Warren CR. 2009. Role of mesophyll diffusion conductance in constraining potential photosynthetic productivity in the field. Journal of Experimental Botany **60**, 2249–2270.

Nunes TDG, Zhang D, Raissig MT. 2020. Form, development and function of grass stomata. The Plant Journal **101**, 780–799.

Pantin F, Simonneau T, Muller B. 2012. Coming of leaf age: control of growth by hydraulics and metabolics during leaf ontogeny. New Phytologist **196**, 349–366.

Papanatsiou M, Petersen J, Henderson L, Wang Y, Christie J, Blatt M. 2019. Optogenetic manipulation of stomatal kinetics improves carbon assimilation, water use, and growth. Science **363**, 1456–1459.

Pearcy RW. 1990. Sunflecks and photosynthesis in plant canopies. Annual Review of Plant Physiology **41**, 421–453.

Pearcy RW, Gross LJ, He D. 1997. An improved dynamic model of photosynthesis for estimation of carbon gain in sunfleck light regimes. Plant, Cell & Environment **20**, 411–424.

Pearcy RW, Krall JP, Sassenrath GF. 1996. Photosynthesis in fluctuating light environments. In: Baker NR, ed. Photosynthesis and the environment. Dordrecht: Springer, 321–346.

Porra RJ, Thompson WA, Kriedemann PE. 1989. Determination of accurate extinction coefficients and simultaneous equations for assaying chlorophylls *a* and *b* extracted with four different solvents: verification of the concentration of chlorophyll standards by atomic absorption spectroscopy. Biochimica et Biophysica Acta **975**, 384–394.

Qu M, Hamdani S, Li W, *et al*. 2016. Rapid stomatal response to fluctuating light: an under-explored mechanism to improve drought tolerance in rice. Functional Plant Biology **43**, 727–738.

Rengasamy P. 2010*a*. Osmotic and ionic effects of various electrolytes on the growth of wheat. Australian Journal of Soil Research **48**, 120–124.

Rengasamy P. 2010*b*. Soil processes affecting crop production in salt-affected soils. Functional Plant Biology **37**, 613–620.

Richter JA, Behr JH, Erban A, Kopka J, Zorb C. 2019. Ion-dependent metabolic responses of *Vicia faba* L. to salt stress. Plant, Cell & Environment **42**, 295–309.

Sakoda K, Yamori W, Groszmann M, Evans JR. 2021. Stomatal, mesophyll conductance, and biochemical limitations to photosynthesis during induction. Plant Physiology **185**, 146–160.

Sakoda K, Yamori W, Shimada T, Sugano SS, Hara-Nishimura I, Tanaka Y. 2020. Higher stomatal density improves photosynthetic induction and biomass production in Arabidopsis under fluctuating light. Frontiers in Plant Science **11**, 589603.

Shabala S, Munns R. 2017. Salinity stress: physiological constraints and adaptive mechanisms. In: Shabala S, ed. Plant stress physiology. Boston: CABI, 24–63.

Sharkey TD. 2016. What gas exchange data can tell us about photosynthesis. Plant, Cell & Environment **39**, 1161–1163.

Sharkey TD, Bernacchi CJ, Farquhar GD, Singsaas EL. 2007. Fitting photosynthetic carbon dioxide response curves for C_3 leaves. Plant, Cell & Environment **30**, 1035–1040.

Tavakkoli E, Rengasamy P, McDonald GK. 2010. The response of barley to salinity stress differs between hydroponic and soil systems. Functional Plant Biology **37**, 621–633.

Taylor SH, Long SP. 2017. Slow induction of photosynthesis on shade to sun transitions in wheat may cost at least 21% of productivity. Philosophical Transactions of the Royal Society of London, Series B: Biological Sciences **372**, 20160543.

Termaat A, Munns R. 1986. Use of concentrated macronutrient solutions to separate osmotic from NaC1-specific effects on plant growth. Australian Journal of Plant Physiology **13**, 509–522.

Tinoco-Ojanguren C, Pearcy RW. 1993. Stomatal dynamics and its importance to carbon gain in two rain forest *Piper* species. II. Stomatal versus biochemical limitations during photosynthetic induction. Oecologia **94**, 395–402.

Trouwborst G, Hogewoning SW, Harbinson J, van Ieperen W. 2015. The influence of light intensity and leaf age on the photosynthetic capacity of leaves within a tomato canopy. Journal of Horticultural Science and Biotechnology **86**, 403–407.

Urban O, Šprtová M, Košvancová M, Tomášková I, Lichtenthaler HK, Marek MV. 2008. Comparison of photosynthetic induction and transient limitations during the induction phase in young and mature leaves from three poplar clones. Tree Physiology **28**, 1189–1197.

Valladares F, Allen MT, Pearcy RW. 1997. Photosynthetic responses to dynamic light under field conditions in six tropical rainforest shrubs occuring along a light gradient. Oecologia **111**, 505–514.

van Delden SH, Nazarideljou MJ, Marcelis LFM. 2020. Nutrient solutions for *Arabidopsis thaliana*: a study on nutrient solution composition in hydroponics systems. Plant Methods **16**, 72.

Vialet-Chabrand SRM, Matthews JSA, McAusland L, Blatt MR, Griffiths H, Lawson T. 2017. Temporal dynamics of stomatal behavior: modeling and implications for photosynthesis and water use. Plant Physiology **174**, 603–613.

Wang Y, Burgess SJ, de Becker EM, Long SP. 2020. Photosynthesis in the fleeting shadows: an overlooked opportunity for increasing crop productivity? The Plant Journal **101**, 874–884.

Wang X, Wang W, Huang J, Peng S, Xiong D. 2017. Diffusional conductance to CO_2 is the key limitation to photosynthesis in salt-stressed leaves of rice (*Oryza sativa*). Physiologia Plantarum **163**, 45–58.

Wang Y, Hills A, Vialet-Chabrand S, Papanatsiou M, Griffiths H, Rogers S, Lawson T, Lew VL, Blatt MR. 2017. Unexpected connections between humidity and ion transport discovered using a model to bridge guard cell-to-leaf scales. The Plant Cell **29**, 2921–2939.

Wu BJ, Chow WS, Liu YJ, Shi L, Jiang CD. 2014. Effects of stomatal development on stomatal conductance and on stomatal limitation of photosynthesis in *Syringa oblata* and *Euonymus japonicus* Thunb. Plant Science **229**, 23–31.

Wungrampha S, Joshi R, Singla-Pareek S, Pareek A. 2018. Photosynthesis and salinity: are these mutually exclusive? Photosynthetica **56**, 366–381.

Xiong D, Douthe C, Flexas J. 2018. Differential coordination of stomatal conductance, mesophyll conductance, and leaf hydraulic conductance in response to changing light across species. Plant, Cell & Environment **41**, 436–450.

Yamori W, Kusumi K, Iba K, Terashima I. 2020. Increased stomatal conductance induces rapid changes to photosynthetic rate in response to naturally fluctuating light conditions in rice. Plant, Cell & Environment **43**, 1230–1240.

Zhang Y, Kaiser E, Marcelis LFM, Yang Q, Li T. 2020. Salt stress and fluctuating light have separate effects on photosynthetic acclimation, but interactively affect biomass. Plant, Cell & Environment **43**, 2192–2206.

Zhang Y, Kaiser E, Zhang Y, Yang Q, Li T. 2018. Short-term salt stress strongly affects dynamic photosynthesis, but not steady-state photosynthesis, in tomato (*Solanum lycopersicum*). Environmental and Experimental Botany **149**, 109–119.

Zhang Q, Peng S, Li Y. 2019. Increase rate of light-induced stomatal conductance increase rate is related to stomatal size in the genus *Oryza*. Journal of Experimental Botany **70**, 5259–5269.

Zipperlen SW, Press MC. 1997. Photosynthetic induction and stomatal oscillations in relation to the light environment of two dipterocarp rain forest tree species. Journal of Ecology **85**, 491–503.